Science Bulletin 64 (2019) 843–855

Contents lists available at ScienceDirect

Science Bulletin

journal homepage: www.elsevier.com/locate/scib

Review

Integrated spoof plasmonic circuits

Jingjing Zhang, Hao-Chi Zhang, Xin-Xin Gao, Le-Peng Zhang, Ling-Yun Niu, Pei-Hang He, Tie-Jun Cui *

State Key Laboratory of Millimeter Waves, Southeast University, Nanjing 210096, China

ARTICLE INFO

Article history:
Received 30 November 2018
Received in revised form 21 January 2019
Accepted 23 January 2019
Available online 2 February 2019

Keywords:
Spoof surface plasmons
Metamaterial
Electromagnetic system
Integrated circuits

ABSTRACT

Using a metamaterial consisting of metals with subwavelength surface patterning, one can mimic surface plasmon polaritons (SPPs) and achieve surface waves with subwavelength confinement at microwave and terahertz frequencies, thus bringing most of the advantages associated with the optical SPPs to lower frequencies. Due to the properties of strong field confinement and high local field intensity, spoof SPPs have demonstrated the improved performance for data transmission and device miniaturization in an intensively integrated environment. The distinctive abilities, such as suppression of transmission loss and bending loss, and increase of signal integrity, make spoof SPPs a promising candidate for future generation of electronic circuits and electromagnetic systems. This article reviews the progress in spoof SPPs with a special focus on their applications in circuits from transmission lines to passive and active devices in microwave and terahertz regimes. The integration of versatile spoof SPP devices on a single platform, which is compatible with established electronic circuits, is also discussed.

1. Introduction

The development of current integrated circuits is now facing several challenges, such as compactness, bandwidth, loss in the transmission of signals, gain, etc. In particular, in dense circuits with multiple layers and a large number of parallel transmission lines, the reduction of the distance between the layers and transmission lines drastically increases the mutual effects between the neighboring components. Moreover, at high operating frequencies the current flow in the circuit tends to crowd towards the surface of metal due to the proximity effect, leading to high ohmic loss as well as large electromagnetic (EM) coupling. Thus, the establishment of signal integrity over a broad band as well as suppression of crosstalk between wirings is among the most critical problems in integrated circuits with high packaging density or at high speed/frequency.

Surface plasmon polaritons (SPPs), defined as collective oscillations of the delocalized electrons in the metal-dielectric interface, offer a promising approach to the miniaturization of electro-optical components for highly integrated circuits, owing to their ability to confine EM waves in a subwavelength scale with high intensity. However, in longer-wavelengths, such as the far-infrared, terahertz, and microwave frequency bands, although conductors can also support EM surface waves, metals behave akin to perfectly electrical conductors (PECs) and the fields are only weakly confined in the dielectric [1–3]. Surface patterning of metal, such as arrays of holes or grooves, can increase the penetration of the field into the metal and thus the binding of surface waves [4,5]. In 2004, this idea was further studied with effective medium theory and the concept of "spoof SPPs" was firstly suggested [6]. With a metamaterial consisting of metal surfaces textured with subwavelength periodic features, one can mimic surface plasmons at much shorter wavelengths and achieve surface waves with subwavelength confinement at infrared wavelengths and beyond. As shown in Fig. 1, the SPP dispersion and spatial confinement can be controlled by means of surface patterning. For a 2D array of square holes with the size of $(a \times a)$ and the spacing (d), where a and d are much smaller than the wavelength, the dispersion relation can be obtained as

$$k_{\mathrm{ssp}}^2 c_0^2 = \omega^2 + \frac{1}{\omega_{\mathrm{pl}}^2 - \omega^2} \frac{64 a^4 \omega^4}{\pi^4 d^4}, \tag{1}$$

where k_{ssp} is the transverse wave vector of surface waves propagating along the metal layer, and ω_{pl} is the plasma frequency for the effective medium.

$$\omega_{\mathrm{pl}} = \frac{\pi c_0}{a\sqrt{\varepsilon_{\mathrm{h}} \mu_{\mathrm{h}}}}, \tag{2}$$

where c_0 is the speed of light in free space, and ε_{h} and μ_{h} are the permittivity and permeability of the material filling the holes, respectively.

SPECIAL TOPIC: Electromagnetic Metasurfaces: from Concept to Applications.

* Corresponding author.
E-mail address: tjcui@seu.edu.cn (T.-J. Cui).

https://doi.org/10.1016/j.scib.2019.01.022
2095-9273/

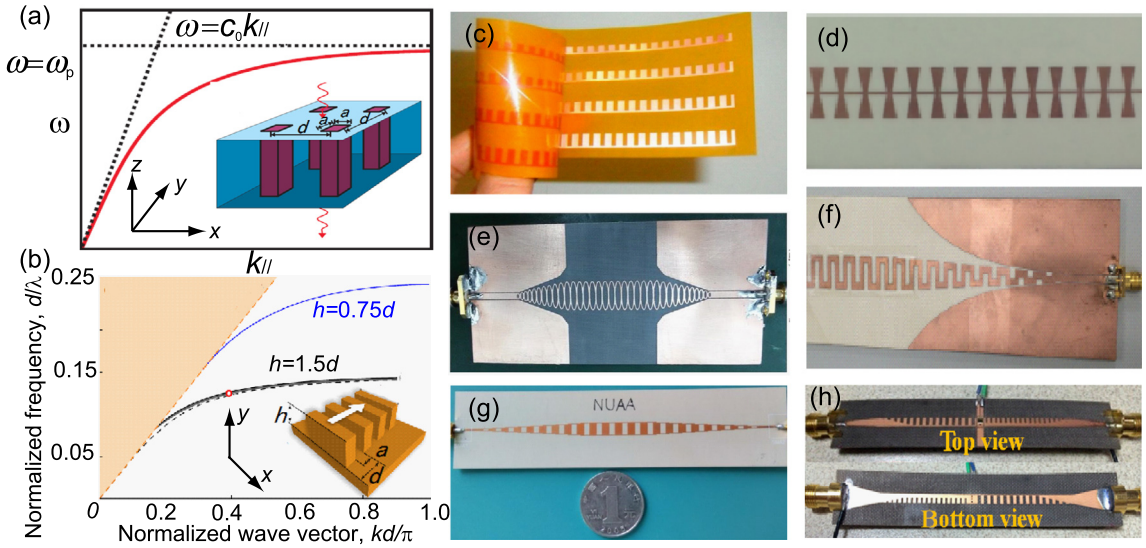

Fig. 1. Metamaterial description of spoof SPPs on corrugated metal surfaces. (a) Schematic diagram of a 2D array of holes and the associated dispersion relation. Reproduced with permission [6], Copyright (2004) AAAS. (b) Schematic diagram of a 1D array of grooves and the associated dispersion relation. Reproduced with permission [7], Copyright (2010), OSA. (c) Single-side spoof SPP TL printed on a flexible and ultrathin substrate. Reproduced with permission [8], Copyright (2013), National Academy of Sciences. (d) Spoof SPP TL consisting of trapezoidal grooves. Reproduced with permission [9], Copyright (2015), AIP. (e) Spoof SPP TL consisting of oval-ring shaped cells. Reproduced with permission [10], Copyright (2018), NPG. (f) Spoof SPP TL with meander slots. Reproduced with permission [11], Copyright (2016), IEEE. (g) Spoof SPP TL consisting of gradient holes. Reproduced with permission [12], Copyright (2015), AIP. (h) Anti-symmetric spoof SPP TL. Reproduced with permission [13], Copyright (2016), ACS.

A 1D array of grooves perforated on a PEC surface where the width, depth, and the periodicity of the groove are a, h and d, respectively, the dispersion relation is given by [14]

$$\frac{\sqrt{k_{ssp}^2 - k_0^2}}{k_0} = \frac{a}{d}\tan(k_0 h). \tag{3}$$

The existence of such spoof SPPs was experimentally observed in 1D [15–17] and 2D [18–21] configurations at microwave and terahertz frequencies. This metamaterial approach allows the transfer of most of the advantages associated with optical SPPs to lower frequencies. In particular, spoof SPP devices can achieve higher efficiency and longer propagation length as compared to conventional SPP devices due to the low loss of metal in terahertz and microwave spectra. Moreover, the performance of spoof SPP devices can be engineered by tuning the geometry of the surface patterning, thus giving us extended freedom in the device design. However, the bulky structures of all the above-mentioned plasmonic metamaterials limit their applications, especially in electronic and photonic circuits where compactness is highly desired. The inherent 3D design with dimensional structure vertically below/above the conducting surface makes those plasmonic metamaterials impossible to integrate with electronic devices or components. As a solution to this issue, an ultrathin form of spoof SPP transmission line (TL) was proposed, where EM waves can be confined in the subwavelength scale and can propagate on flexible and curved surfaces [8,22]. This conformal spoof SPP TL can be fabricated with the standard printed circuit board technology. Fig. 1c shows the first experimental demonstration of an ultrathin conformal spoof SPP TLs printed on a flexible film, where the propagation of confined spoof SPPs can adapt to the curvature of the surface [8]. Following this innovative work, TLs engraved with a variety of different ultrathin structures have been developed to support spoof SPPs, such as the trapezoidal grooves [9], oval-ring shaped cells [10], and meander slots [11], as shown in Fig. 1d–f. Dual-band trapping of spoof SPPs can be achieved through a microstrip line with periodic holes [12], as shown in Fig. 1g. Recently, anti-symmetric spoof SPP TLs, which can be integrated with active devices have been reported as well [13], as shown in Fig. 1h.

One challenge of applying the spoof SPP TLs in circuit design lies in the feeding of the TLs and the conversion from conventional circuits to spoof SPP devices so that the efficiency and bandwidth can be maximized. Extensive studies have been performed on this topic, and different techniques have been proposed at both microwave [23–27] and sub-terahertz [28] frequencies. Owing to the high field confinement property, the conformal spoof SPs do not suffer from the compactness limitations of traditional circuits. The near zero thickness, great flexibility, and easy fabrication feature make this new type of TL a promising candidate for the high-speed communication devices in the modern era of electronics.

In the following, we review the development of spoof SPP devices and systems based on spoof SPP TLs. We begin by summarizing the advantages of spoof SPP TLs over the traditional TLs. Next, we introduce the development of effective circuit models for spoof SPP TLs and analyze the arising challenges in treating practical cases. Then, we give a detail review of the diverse implementations of passive and active spoof SPP devices. Finally, we envision the integration of the spoof SPP devices of different functions on a single platform, which is compatible with established electronic circuits. Potential new applications and research directions are also outlined.

2. Advantages of spoof SPP TLs over conventional TLs

Table 1 summarizes the comparison between spoof SPP TLs and conventional microstrip lines, in terms of cross talk suppression, transmission loss and bending loss reduction, and the miniaturization feature. The interference between adjacent signals is almost inevitable when two transmission lines are tightly packed with deep-subwavelength separation in conventional integrated circuits. In order to overcome this problem, a special spoof SPPs TL has been proposed in Ref. [29], where two narrow corrugated metallic strips are printed on the top and bottom surfaces of a dielectric substrate with mirror symmetry. It has been demonstrated theoretically and experimentally that the signals on such two spoof SPPs TLs have better propagation performance and much less mutual coupling than the conventional signals on two tradi-

Table 1
Performance comparison between the spoof SPPs transmission line and the conventional microstrip line.

Performance	Spoof SPPs transmission line	Microstrip line	Reference
Adjacent mutual coupling coefficients (>5 GHz)	<–15 dB	>–15 dB –5 dB (max)	Ref. [29]
Transmission coefficients $\mathbf{S_{21}}$ (3–9 GHz)	–3 dB (average) –2 dB (max)	–6 dB (average) –3 dB (max)	Ref. [30]
Bending transmission coefficients $\mathbf{S'_{21}}$ (5–10 GHz)	–1.5 dB (average)	–2 dB (average)	Ref. [31]
Reflection coefficient $\mathbf{S_{11}}$ with shielding-box structure (5–15 GHz)	≈ –10 dB	≈ –4 dB	Ref. [32]

tional microstrip lines with the same size and separation. In Ref. [29], the crosstalk in the spoof SPPs TLs is lower than –15 dB from 5 to 20 GHz, while that of a conventional microstrip line is higher than –15 dB even up to –5 dB. Hence, the spoof SPPs TLs can achieve significant interference suppression in very compact space. In Ref. [33], two kinds of spoof SPP TLs are proposed based on differential microstrip lines with subwavelength periodic corrugations. The EM fields can be tightly confined inside the corrugations and therefore, the crosstalk between the differential pair and the adjacent microstrip lines can be effectively suppressed as compared to conventional microstrip lines. The transmission coefficient in the spoof SPPs TLs with unilateral periodic corrugations is about –2.91 dB at 12 GHz, while that of the microstrip line is about –4.88 dB. Spoof SPP TLs have also been applied at subterahertz frequencies to improve the signal integrity [34]. Two on-chip SPP TLs are back-to-back placed so that the crosstalk between them is significantly reduced. Compared with two traditional quasi-TEM TLs with line space of 2.4 μm in a standard 65 nm CMOS process, the spoof SPP TL can achieve a wideband reflection coefficient lower than –14 dB and the crosstalk ratio better than –24 dB, which is 19 dB lower on average than that of the traditional T-lines from 220 to 325 GHz.

Transmission loss is another critical issue which may significantly deteriorate the performance of the electronic system, and spoof SPP provides a method to cope with this problem. In contrast to conventional microstrip lines in which the coupling coefficient increases with the propagation constant, the spoof SPPs offer tighter field confinement as the propagation constant is increased, making the transmission power insensitive to the coupling length [29]. A method based on the designable wavenumber of spoof SPPs TLs is proposed in Ref. [30] to reduce the loss of microwave transmission line. Through the perturbation method and *S*-parameter measurements, both simulation and experimental results show that the spoof SPPs TLs have much smaller transmission loss than traditional microstrips with the same size within the operating frequency range. The transmission coefficient in the spoof SPPs TLs is about –3 dB in average from 3 to 9 GHz, while that of microstrip line is about –6 dB, as shown in Table 1. In Ref. [35], in order to overcome the problem of large metallic losses and short propagation length, the concept of dielectric spoof SPPs and subwavelength high-contrast gratings was introduced. A wideband ultra-low-loss high-confinement plasmonic waveguide is experimentally realized with a high refractive-index dielectric array with deep-subwavelength periodicity on a metal substrate. Simulation and measurement results on the nearfield distributions and *S*-parameters demonstrate the excellent transmission efficiency across a broad frequency band.

The reduction of bending loss is another common problem in highly-integrated circuits or systems. Ref. [36] demonstrates theoretically that the bending loss can be effectively reduced by increasing the confinement of EM fields in the spoof SPP TLs. Thus, the metamaterial feature offers us the freedom of achieving this goal by tuning the geometrical parameters of the spoof SPP structure. In Ref. [31], the suppression of radiation loss at small-radius bend of spoof SPPs TLs by 0.5 dB from 5 to 10 GHz is experimentally demonstrated.

The shielding-box technology is proposed to overcome the problem of external disturbance in most modern electrical circuits and systems. However, for traditional microwave planar transmission lines, it is very difficult to reduce the volume of the shielding-box. In Ref. [32], a method is proposed to reduce the shielding-box volume based on the tight field confinements of spoof SPPs TLs. As demonstrated theoretically and experimentally, the EM signals on spoof SPP TLs have better propagation performance than those on traditional microstrip lines with the same size and separation to the shielding box. The reflection coefficient with shielding-box structure of the spoof SPPs TLs is about –10 dB from 5 to 15 GHz, as compared to the microstrip line of which the reflection coefficient is about –4 dB [32], thus providing a potential solution to the miniaturization of metallic package.

3. Effective circuit model of spoof SPP TLs

The design and optimization of spoof SPP TL associated devices require a theoretical model that can characterize the transmission of EM waves in the spoof SPP TLs. In traditional microwave circuit engineering, the effective circuit model of the transmission structure is one of the most important stepping-stones to analyze and synthesize the microwave device and system. However, different from the traditional homogeneous TL (i.e. the microstrip, coplanar waveguide, and so on), the spoof SPPs TL is a new type of inhomogeneous TL, whose impedance is dependent on the location in the propagation direction. In order to overcome this difficulty, the concepts of the Bloch wavenumber and impedance is used to replace the original wavenumber and impedance concept, respectively, based on the fact that the Bloch wavenumber and impedance can be directly obtained through the analysis on the unit of the spoof SPP TL.

To obtain the Bloch wavenumber and impedance of the ultrathin corrugated metallic strip, the mode matching method from the field view is firstly investigated in Ref. [37], where an analytical solution is given for the ultrathin corrugated metallic strip. The field view indicates that this mode results from the resonance between the metallic structure and the EM wave around. However, this method cannot be used to describe the case that the strip is integrated with the dielectric substrate, which is commonly used in real applications. In order to solve this problem, the effective circuit model is introduced to describe the EM behavior of the spoof SPPs from the circuit view [26,38–41]. In Refs. [26,38,39], the unit structure is dismembered as the metallic patches and grooves between the metallic patches, and they are further considered as inductors and capacitors based on the low frequency approximation, as shown in Fig. 2a. The dispersion curve of this structure can thus be qualitatively described by this lumped circuit model, and is gradually deviating from the light line and approaching to the cut-off frequency.

From the circuit view, the slow-wave properties of the spoof SPPs transmission line is led by the phase delay caused by resonance oscillation between the lumped capacitors and lumped inductors. However, the calculated dispersion curve based on the lumped model does not quantitatively agree with the simulated result, resulting from ignoring the spatial dispersion of the

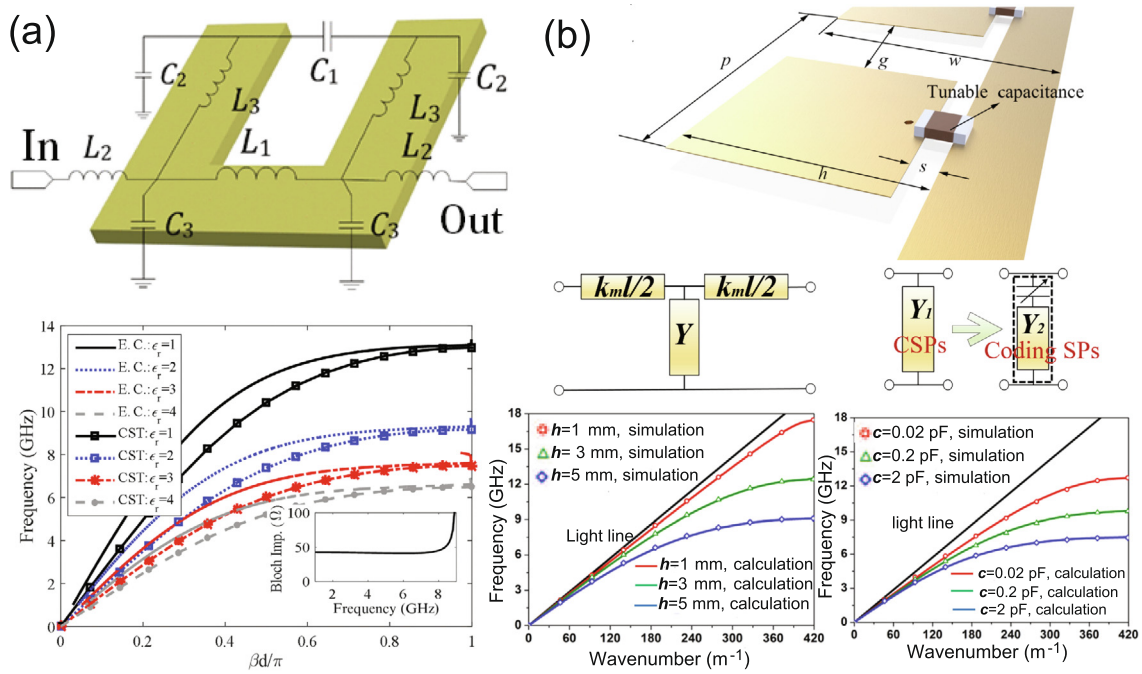

Fig. 2. Schematic structures and effective circuit topologies of the spoof SPPs TLs. (a) The schematic structure, relative effective lumped circuit topologies, and dispersion curve of the common corrugated metallic strip. Reproduced with permission [26], Copyright (2015), IEEE. (b) The schematic structure, relative effective transmission line circuit topologies, and dispersion curves of active spoof SPPs transmission line. Reproduced with permission [41], copyright (2017), Wiley-VCH.

structure. Hence, as an improvement scheme, the transmission line model is introduced into the circuit topology. Furthermore, some lumped-distributed integrated model is also developed to improve the accuracy [41–45]. Ref. [41] introduced an active spoof SPPs transmission line structure, whose EM behavior can be controlled in real-time coding sequence, as shown in Fig. 2b. Different from the lumped circuit model, the series branch and the shunt branch are regarded as a planar Goubau line [46] and an open CPW, respectively, due to the coupling between adjacent unit cells. Furthermore, a tuning capacitance is introduced into the front end of the shunt branch of the structure to obtain the ability of controllable performance.

As shown in Fig. 2b which displays the dispersion curves of active spoof SPPs transmission line with different length and capacitance, the calculated results have very good agreement with the simulated result, indicating that the transmission line circuit model provides a possible bridge between spoof SPPs TLs and the design of microwave devices. By comparing the lumped and transmission line models, we can find that the improvement of the calculation accuracy can be achieved by taking account of the spatial dispersion, namely, describing the metallic structure as the dispersive capacitances and inductance instead of the original lumped elements. Moreover, by introducing the attenuation constant into the distributed structure, the lumped-distributed integrated model can be applied to further analyze the loss properties, which cannot be treated through the common lumped model and the commercial simulation software, such as CST microwave studio and Ansys HFSS. However, for complex cases, the lumped-distributed model still has some challenges to overcome: (1) the method to deal with the coupling of adjacent structure; (2) the possible high-order mode around the discontinuous structure.

4. Passive spoof SPP devices

TL is a key element in data transmission and the basis for all kinds of devices in integrated circuits. The theoretical models of spoof SPP TLs thus provide a useful guidance for the design and experimental demonstration of passive and active spoof SPP devices. The distinctive features of spoof SPPs enable the realization of a variety of devices for modern electronics, ranging from filters, couplers to resonators and antennas, with improved performance compared to traditional devices.

4.1. Resonator based on spoof SPPs

In 2012, the concept of spoof plasmonics was transplanted to localized surface plasmons (LSPs) [47]. By texturing closed surfaces, a finite metal structure is shown to support multiple surface modes, resembling natural LSPs [48–50] at optical frequencies. This powerful approach enables the realizations of various spoof LSP resonators [51–57], which have been widely used in sensing [51,58], filtering [22,59–61], dispersion control [44,62], etc. A typical example is the fan-shaped plasmonic ring resonator [51], as shown in Fig. 3a. The resonance frequencies can be controlled by properly designing the inner and outer radii of the structure. In the experiment, multipolar surface modes were observed, as shown in Fig. 3b.

Spoof LSPs have several advantages over their optical counterparts. First, they can be applied to the design of deep-subwavelength resonators at low frequencies. Fig. 3c depicts one of such examples realized in previous work [55], where the spiral shape of the structure enables the accommodation of longer corrugations within the same area. Consequently, the effective capacitance of the structure is significantly increased and the resonance frequency is dramatically decreased. The extinction and field spectra plotted in Fig. 3d clearly demonstrate the low-loss and subwavelength properties of the structure. Another advantage of spoof LSPs is related to their conformal feature, where the extremely strong interaction between two vertically orientated resonators (see Fig. 3e) enables the observations of the many interesting phenomenon difficult to realize with natural LSPs. Fig. 3f illustrates one of such examples, where the strong coupling between the hexapole and octopole leads to the observation of "invisibility dip" [50,63] in the near-field spectrum. Spoof LSP reso-

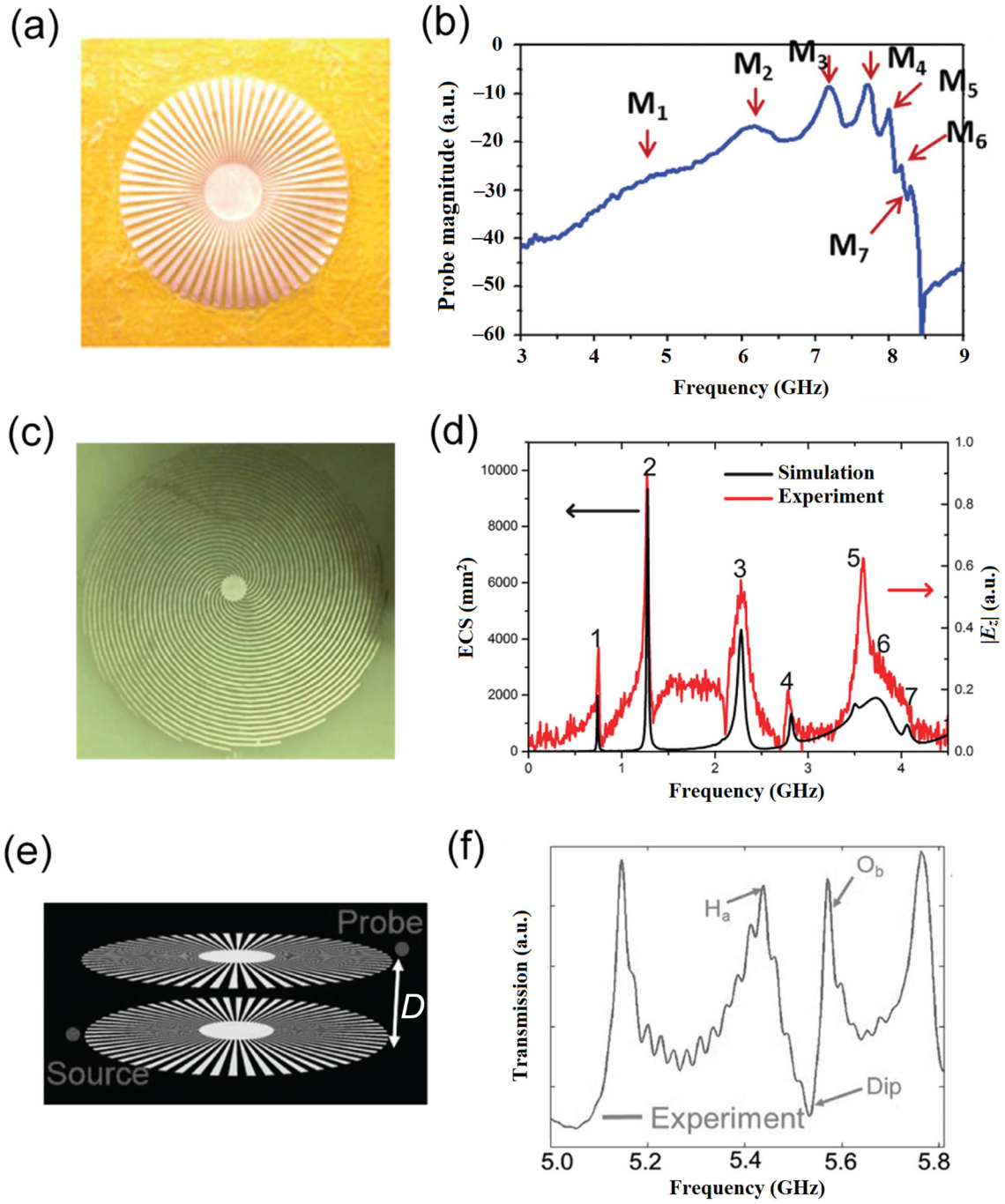

Fig. 3. (a) and (b) The fabricated samples of spoof LSP resonators and the corresponding spectra for single-layer fan-shaped resonator, Reproduced with permission [51], Copyright (2014), Wiley-VCH. (c) and (d) single-layer spiral resonator, Reproduced with permission from Ref. [55], Copyright (2016), ACS. (e) and (f) double-layer fan-shaped resonator. Reproduced with permission [58], Copyright (2016), Wiley-VCH.

nances are very sensitive to the local dielectric environments, thus providing promising solutions for refractive-index sensing with high sensitivity [51,64]. Numerical and experimental studies have demonstrated that higher order modes exhibited better sensitivity [54,55], and a tunable spoof LSP structure with a ground plane has been proposed to achieve higher-order azimuthal resonance modes with improved *Q* factor and sensitivity [64].

4.2. Filters based on spoof SPPs

In order to remove harmonics in electronic devices and communication systems, the filters based on spoof SPPs are widely studied, particularly the passive devices including the band-stop filters and the band-pass filters. In terms of the band-stop filter, changing the several groove structures of spoof SPP TL or utilizing the resonant metamaterials as well prevents the EM wave transmission in specific frequency ranges [59–61,65–69]. Ref. [60] proposes a band-stop filter, whose bottom structure is designed as CPW and the top is designed as the corrugated metallic strip with nine defects arranged every three periods. The defects can form a broadband CPW band-stop filter and the center frequency and bandwidth can be tuned by the height and numbers of the defect units. Another band-stop filter is designed by placing a conventional microstrip at the bottom center of a double sided spoof

SPP TL with defects of variable dimension [61], and a band-rejection filter is implemented by loading split-ring resonators embeded on the spoof SPP TL [65]. Ref. [66] introduces the tunable frequency- rejection filter using the resonant metamaterials near the spoof SPP TLs to produce tight coupling and mismatch of the surface impedance. Ref. [67] proposes a spoof SPP band-stop filter by using several two H-shaped unit cells separated by a gap to implement capacitive coupling and further lead to the stopband of spoof SPP TL. Fig. 4 shows the structure of band-rejection filter by etching split-ring resonators (SRRs) on spoof SPP transmission

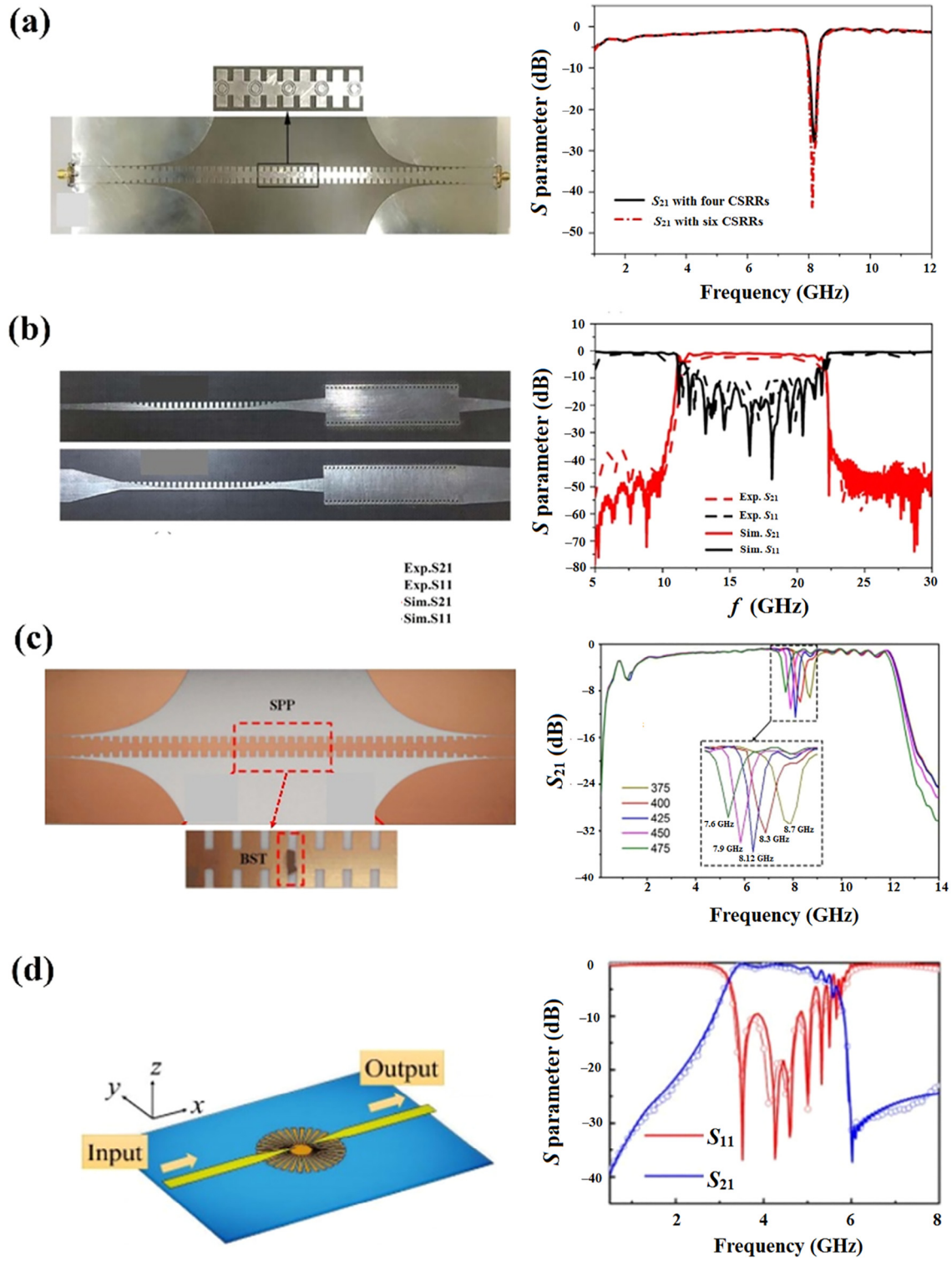

Fig. 4. The sample and *S*-parameters of filters based on spoof SPPs. (a) The schematic of the rejection filters based on the interaction between spoof SPPs and complementary split-ring resonators (CSRRs) and the simulated results with four CSRRs (black line) and six CSRRs (red line). Reproduced with permission [68], Copyright (2016), NPG. (b) The structures of the front and back surfaces of the SPP-SIW hybrid circuits and the measured and simulated results of *S*-parameters. Reproduced with permission [70], Copyright (2015), NPG. (c) The photograph of a spoof SPP filter with the tunable high-permittivity dielectric block BST and the transmission coefficient under different BST dielectric constants. Reproduced with permission [69], Copyright (2018), IEEE. (d) Schematic of the spoof localized surface plasmon filter and the simulated and measured S-parameters. Reproduced with permission [71], Copyright (2018), Wiley-VCH.

line [68]. The complementary SRRs (CSRRs) lead to resonant modes and further prevent the SPP propagation. Simulated results show that the band-rejection effect is more obvious as the number of CSRRs increases. When 6 CSRRs are etched, the transmission coefficient is lower than –40 dB, which is almost totally cutoff. A novel tunable SPP filter is implemented [69], where the corrugated metallic and tuning permittivity material is utilized to change the transmission state. As shown in Fig. 4c, the BST dielectric block, whose dielectric constant is sensitive to temperature and the applied electric field, is embedded into a gap of spoof SPP TL with tuning permittivity. As the dielectric constant of BST increases from 375 to 475, the notch frequency shifts from 8.7 to 7.6 GHz.

For the band-pass filter, changing the groove structure of spoof SPP TL or adding extra structure can control the transmission frequency [70–75]. Ref. [72] proposes an ultra-wideband filter by using a double side spoof SPP TL decorated with parallel arranged slots. Introducing parallel arranged slots enhances subwavelength field confinement and further construct miniaturization. A tunable band-pass filter, based on spoof SPP TL and the substrate integrated waveguide (SIW), has been reported in Ref. [70]. As shown in Fig. 3b, the hybrid circuit composing of spoof SPP and SIW can arbitrarily tune the transmission bands by changing their structure parameters, where spoof SPP TL and SIW can adjust the high and low frequency, respectively. Simulated and measured results demonstrate the filter effect of the hybrid circuit, which are high efficiency, low loss, and good square ratio. Ref. [73] also proposes the band-pass filter based on spoof SPPs and SIW, where spoof SPPs are designed to propagate inside the SIW by employing arrays of transverse metallic blind holes. Surface wave mode can be excited and transmitted inside the closed structure of SIW. Similarly, the band-pass filter is implemented by combining the low-pass feature of SPPs with the high-pass feature of SIW. Moreover, other types of filters based on spoof SPPs have also been reported. Ref. [71] introduces a wide band-pass filter based on multipole resonances of spoof localized surface plasmons (LSP) as shown in Fig. 4d. To join discrete multipole resonances into a continuous and flat passband, an interlayer microstrip lines scheme is designed. The working bands of the filter can be controlled by adjusting the geometric parameter of the spoof LSP disk. Simulated and measured results demonstrate the feasibility of the proposed filter, which has the characteristic of compact sizes and well-balanced shaped. Ref. [74] proposes a coplanar waveguide filter by using periodic holes etched on the middle line of the coplanar waveguide, whose merit is removing the mode conversion and more easily integrated at microwave frequencies. Ref. [75] reports another type of band-pass filter, whose lower cutoff frequency controlled by transmission zero that is created by a pair of shunt stepped impedance stubs.

4.3. Splitters and couplers based on spoof SPPs

In order to implement the signal separation and preferably apply the integrated circuits, splitters and couplers are also widely studied. An ultra-wideband Y-splitter based on spoof SPPs is proposed in Ref. [76]. The splitter is composed of a straight waveguide with composite double-side H-shaped structure and two same branches with H-shaped structures, as shown in Fig. 5a. The dispersive relation of the straight waveguide is the same as the two branches structure so that a 3-dB power divider in an ultra-wideband frequency range is implemented. Additionally, a single-conductor coplanar quasi-symmetry unequal power divider (0, 3, and 5 dB) based on spoof SPPs of bow-tie cells has been reported [77].

As shown in Fig. 5b, a variety of power dividers with different structures have been implemented to achieve different power-dividing ratios. The unequal power divider is a flexible option, and an ultrathin frequency splitter composed of a straight complex periodic structure and two branches with the different periodic groove depths has been reported [79]. Note that the complex periodic structure is separated into two branches with single periodic grooves and the splitter is constructed by ultrathin plasmonic metamaterial with the thickness of $\lambda/1600$. Other structure of frequency splitter is reported in Ref. [78]. Based on the coupled mode theory, a 3 dB directional coupler and a frequency splitter are designed by changing the coupling length of two adjacent symmetry spoof SPP TLs. The sample of frequency splitter and the corresponding *S*-parameters are shown in Fig. 4c, where the EM energy can be fully output from port 3 at 3.39 GHz and switched to output port 2 at around 7.42 GHz. As shown in Fig. 5d, a 3 dB directional coupler based on spoof SPP TL is designed. The corresponding *S*-parameters are simulated and measured, where the EM energy from port 1 can be divided equally to port 2 and port 3 from 6 to 9 GHz.

4.4. Antennas based on spoof SPPs

A continuous leaky-wave scanning using periodically modulated spoof plasmonic waveguide has been reported in Ref. [80]. The schematic of leaky-wave antenna based on the spoof SPPs is shown in Fig. 6a. By changing the grooves of the corrugated metallic strip, whose surface impedance is modulated sinusoidally to convert spoof SPPs wave to radiating waves. In both $\Phi = 0^\circ$ and $\Phi = 90^\circ$ planes, the measured far-field radiation angles of E-plane are 63.9° and 43.7° at 8.7 and 9.9 GHz, respectively. Another leaky wave antenna is proposed in Ref. [84], which is composed of a single-layered meander spoof SPP unit cells and the converters between the coplanar waveguide and the spoof SPP structure. As the frequency change, the leaky-wave antenna can generate the radiation space waves with forward, backward and broadside directions. The simulated and measured results show that the leaky-wave antenna has achieved a wide operating bandwidth of 80% and a reflection bandwidth of up to 95%. In addition, frequency-controlled broad angle beam scanning of patch fed by planar spoof SPPs is proposed in Ref. [81].

The schematic of the proposed antenna is shown in Fig. 6b, where the transitional spoof SPP TL is composed of single-side grooves and the array of circularly metallic patches is placed near the spoof SPP TL to form the radiation units. At four different frequencies (6, 7, 8, 9 GHz), simulated and measured results of the far-field radiation patterns of the propose antenna array show that the far-radiation radiation beam changes from the backward to forward directions as the frequency increases. The total scan angle reaches 55° with an average gain level of 9.8 dBi. According to the splitter feeding network for array radiations of spoof SPPs, the radiation antenna is reported [82]. The antenna schematic includes a double-side groove strip and two adjacent branches with the ant-symmetrical structures as shown in Fig. 6c. By loading U-shaped particles, the linear phase modulations can be controlled, allowing the EM energy to radiate into the free space. The measured results show that, at 14 GHz, the broadside far-field radiation patterns for $\Phi = 0^\circ$ and $\Phi = 90^\circ$ has reached effectivity radiation. Ref. [83] proposes a microwave vortex-beam emitter based on spoof SPPs, where the emitter consists of a looped double-layer spoof SPP waveguide and a series of circular patches, as shown in Fig. 6d. Here, the waveguide can transmit EM waves and the patches regarded as the radiation units render the phase shifts owing to resonators. The normalized 3D radiation patterns are calculated particularly for the orbital angular momentum (OAM) mode numbers of $l = -1, 0, 1$ appearing at 5.8, 6.0, 6.3 GHz, respectively. Therefore, the vortex beams are generated at different frequencies using different OAM modes.

A multi-beam antenna based on spoof SPPs mode coupling has been reported in Ref. [85], where the antenna structure consists

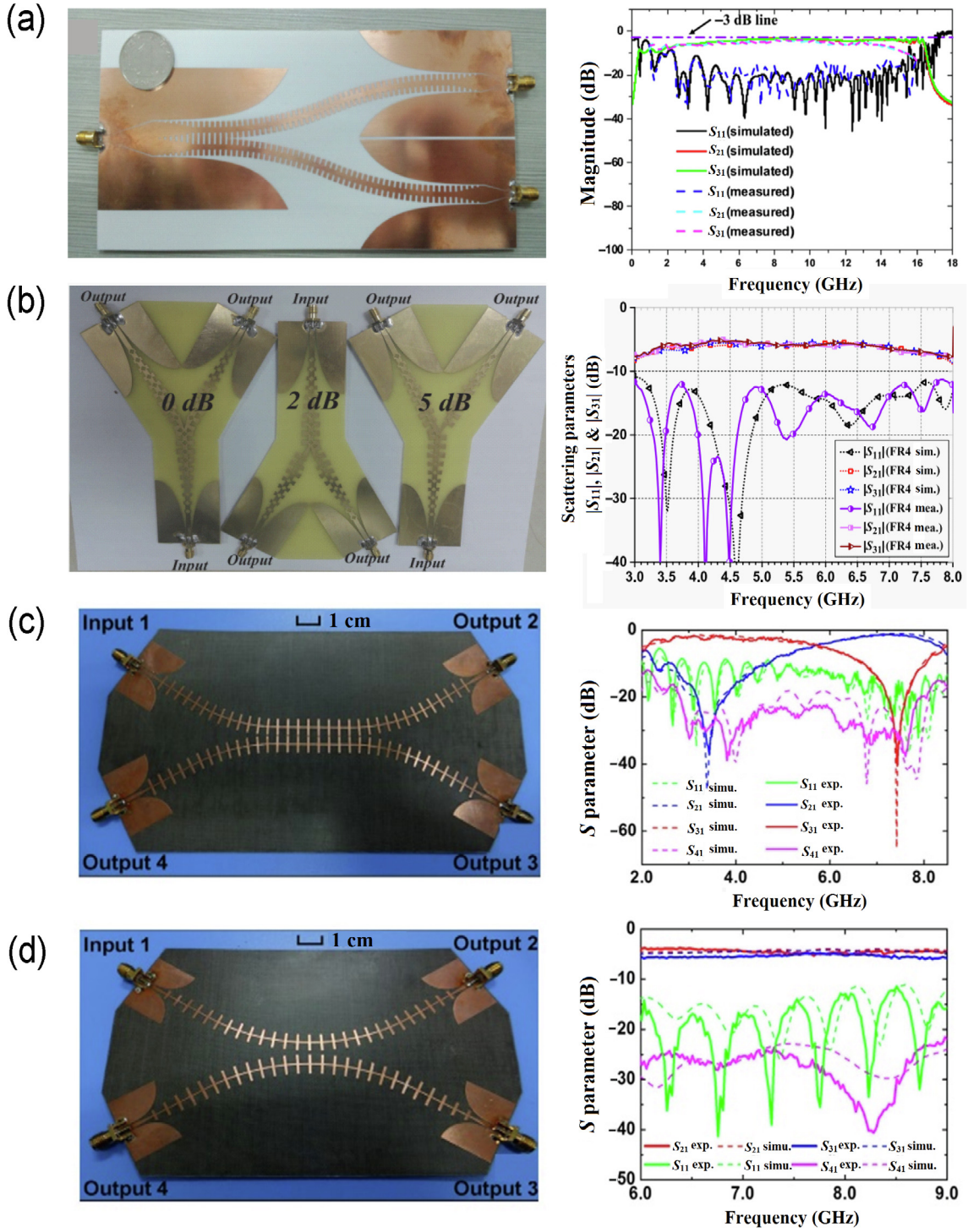

Fig. 5. The samples and *S*-parameters of power dividers and couplers at microwave frequencies. (a) The photograph of the 3 dB spoof SPPs power divider and the simulated and measured *S*-parameters. Reproduced with permission [76], Copyright (2015), OSA. (b) The photograph of the spoof SPPs power dividers and the simulated and measured *S*-parameters of the 0-dB equal power divider. Reproduced with permission [77], Copyright (2016), AIP. (c) The photograph and *S*-parameters of a frequency splitter. Reproduced with permission [78], Copyright (2014), OSA. (d) The photograph and *S* parameters of a 3 dB directional coupler. Reproduced with permission [78], Copyright (2014), OSA.

of a feed monopole and N double-side corrugated metallic strips circling around the feed. The feed fields are coupled into spoof SPP waves propagating along the strips and radiating at the end, which divides the omnidirectional radiation pattern into several beams. Ref. [86] proposes a circularly polarized frequency beam-scanning antenna fed by spoof SPP TL. Eight periodic symmetrical patches as the radiation units at the top layer and spoof SPP TL as the feed network at the bottom layer form the antenna structure. Measured results show that the main beam scans from −5° to +37° in *xoy* plane as the frequency increases (from 12 to 16.5 GHz).

5. Active and real-time control of spoof SPP TL

Active and reconfigurable spoof SPPs have gained increasing attentions and have become a new research direction of spoof SPPs in recent years. The research progress on amplification [87], non-

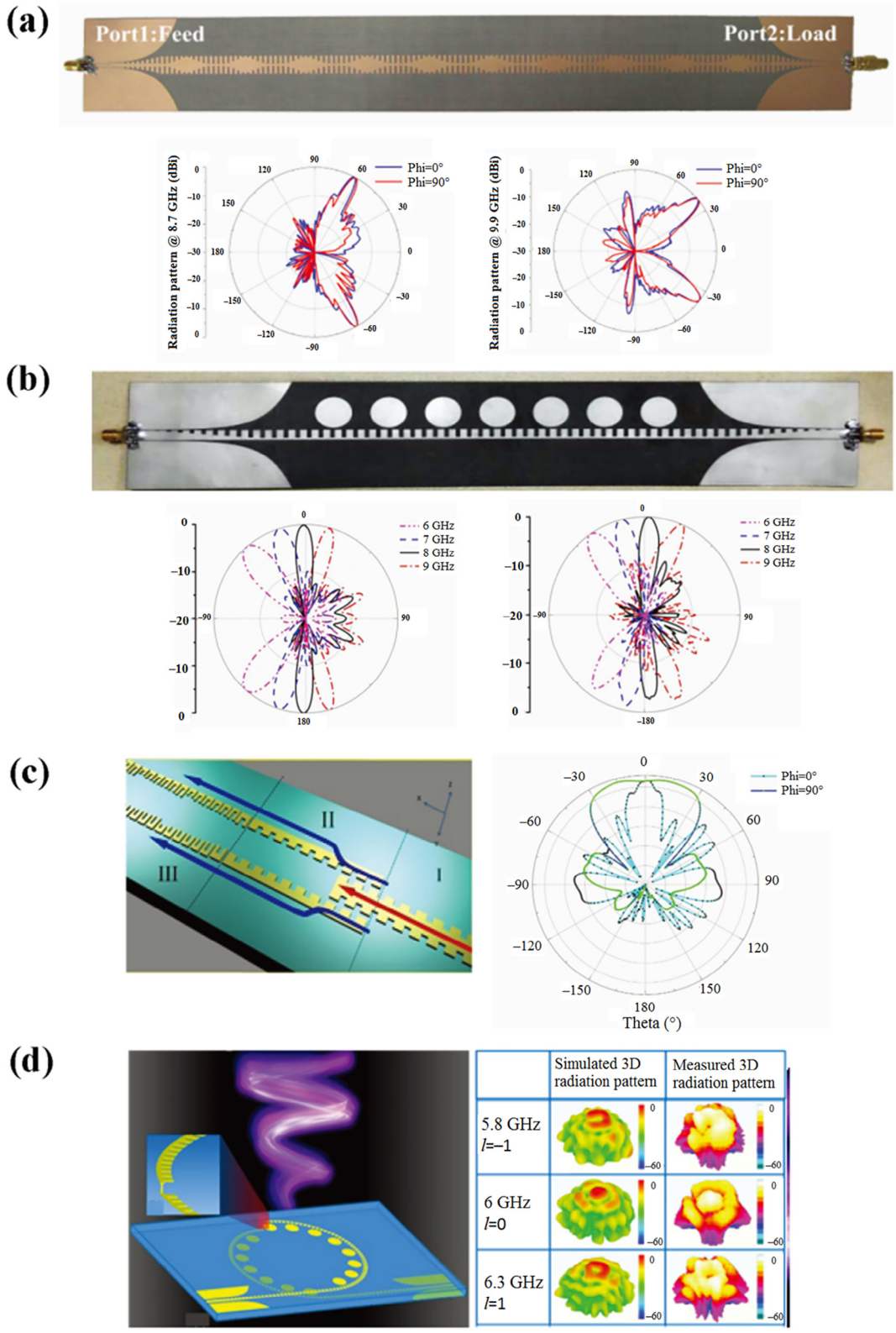

Fig. 6. The fabricated sample and far field radiation pattern of antenna based on spoof SPPs. (a) The photograph of sinusoidally-modulated plasmonic waveguide and the measured far field radiation patterns of E plane in both $\Phi = 0°$ and $\Phi = 90°$ plane at 8.7 and 9.9 GHz. Reproduced with permission [80], Copyright (2016), NPG. (b) Prototype of the spoof SPP-fed antenna array and the simulated and measured far-field radiation patterns at different frequencies. Reproduced with permission [81], Copyright (2016), IEEE. (c) Schematic of the splitter feeding network for array radiation of spoof SPPs and the measured broadside far-field radiation patterns. Reproduced with permission [82], Copyright (2016), NPG. (d) Prototype of the vortex beam emitter and simulated and measured normalized far-field radiation patterns of the OAM modes under different orders. Reproduced with permission [83], Copyright (2018), Wiley-VCH.

linear applications [13,88] and active tuning of spoof SPPs [41,89] are briefly introduced below.

5.1. Amplification and nonlinear applications of spoof SPPs

A subwavelength-scale amplifier has been proposed to amplify the SPP mode at microwave frequencies [87], as shown in Fig. 7a. To easily integrate with the amplifier, two ultrathin corrugated metallic strips with mirror symmetry are printed on the top and bottom surface of dielectric substrate, respectively. Both the simulated and measured results show that transmission coefficient between the input and output ports is around from 6 to 20 GHz. Obviously, the proposed amplifier is a broadband device and has high efficiency and strong field confinement.

Second-harmonic generation is a very important nonlinear application of spoof SPPs [13]. The device shown in Fig. 7b is composed of specially designed plasmonic waveguides mentioned in above amplifier and a subwavelength-scale nonlinear active device integrated on it, and the measured frequency spectrum when the fundamental frequency is 8 GHz is also shown. This device can be used as an SPP frequency multiplier directly.

Fig. 7c shows a negative-index nonlinear spoof plasmonic metamaterial, which can achieve the backward phase matching for efficient SHG [88]. This metamaterial is composed of ultrathin symmetrical corrugated metallic strips loading nonlinear active devices. The spectra from the nonlinear spoof plasmonic metamaterial is measured, where the output signal shows a distinct peak at the double frequency of each excitation frequency.

5.2. Active tuning of SPPs

Programmable designer SPP system provides a novel solution for the active tuning of spoof SPPs [41]. It can reach at least three different digital-analog functions based on the huge freedom of

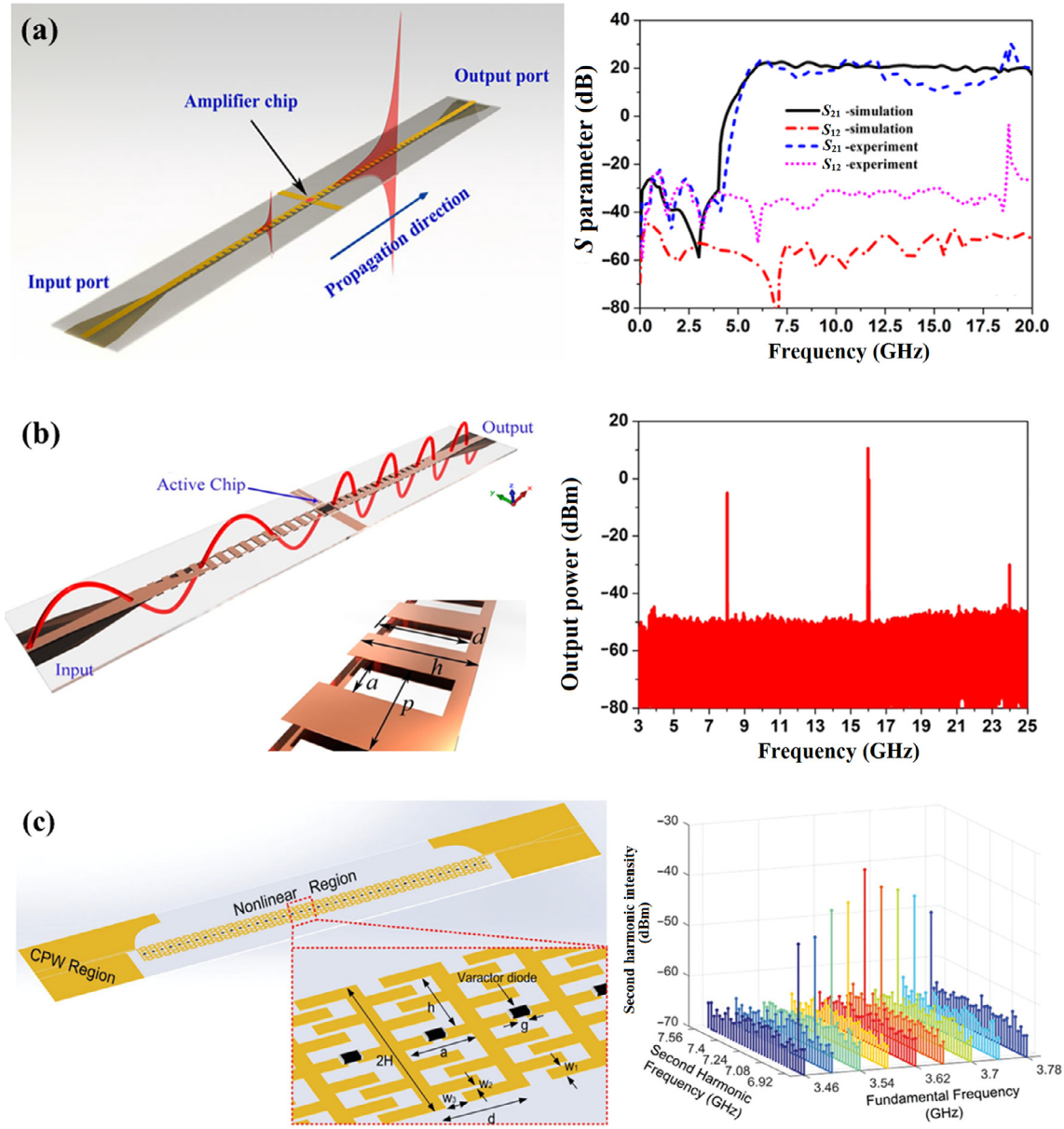

Fig. 7. Amplification and nonlinear applications of spoof SPPs. (a) The physical structure and the simulated and measured scattering *S*-parameters of the SPPs-based amplifier, which is proposed by loading a low-noise amplifier chip onto the anti-symmetric SPPs TL. Reproduced with permission [87], Copyright (2015), Wiley-VCH. (b) The physical structure, which is proposed by loading the nonlinear active elements to the anti-symmetric SPPs TL, and the measured frequency spectrum of the second-harmonic SPP generator when the fundamental frequency is 8 GHz of the second-harmonic generation. Reproduced with permission [13], Copyright (2016), ACS. (c) Negative-index nonlinear spoof plasmonic metamaterial and the spectra of frequency-doubled signals emerging from it. Reproduced with permission [88], Copyright (2018), Wiley-VCH.

coding, including SPP logical gate based on 1-bit coding, SPP digital phase shifter based on 2-bit coding, and controllable slow-wave generations based on 4-bit coding, as shown in Fig. 8a.

A transmission-spectrum-controllable structure [89] which is based on the coupling between tunable metamaterial particles and spoof SPP waveguide is shown in Fig. 8b. Varactor-diodes are introduced into split-ring resonators (SRRs) to tune its resonance frequency, and an inter-digital capacitor is also introduced as the breakpoint of SRR to broaden the dynamic controlling range. Fig. 8c shows a SPP attenuator with ten complicated SPP units [42]. It is obvious that with the increase of complicated SPP units, which perform as cascaded attenuators, the transmission coefficient is reduced rapidly. The measured results show that attenuation reaches −6.3 dB at 5 GHz and −10.7 dB at 6.5 GHz with ten complicated SPPs units. Besides microwave frequencies, the efficient and dynamic steering of spoof SPP waves has also been realized at terahertz frequencies for improved performance in terms of field localization, extinction ratio, and damping attenuation [90].

6. Conclusion and outlook

In this paper, we reviewed the development of spoof SPPs and LSPs from the engineering perspective. Starting with the equivalent circuit models which enable accurate characterizations of the ultrathin spoof SPP and LSP structures and offer the useful guideline for the associated device and circuit designs, we introduced a number of planar passive SPP/LSP devices including the filters, splitters, resonators, antennas, etc., and active and even reconfigurable SPP/LSP devices. Due to the high field confinement property, the spoof SPP/LSP-based TLs and devices do not suffer from the compactness limitation of the conventional microwave technology and have less mutual coupling, thus providing an alternative for future integrated circuits.

The future work in this area on one hand should produce more high-performance passive and active devices, but more importantly needs to make breakthroughs in two directions: system-level applications and CMOS-based integrated circuits [91]. Taking the advantages of spoof SPP/LSP TLs, passive and active devices, an integration study of SPP/LSP systems is highly demanded to reach new technologies of the wireless communications, radar, and EM compatibility. However, such integration is not simply putting the passive and active SPP/LSP devices together. Instead, we need to develop a general method to synthesize and design the whole system. Though the current theoretical framework of TL method is helpful for the system design, it still has some technical difficulties to overcome in the future. For example, how to achieve the equivalent capacitance and inductance with arbitrary values through changing the length of the spoof SPP TL? Apparently, we cannot choose arbitrary lengths of SPP TLs like those in the traditional TLs due to the periodic structural characteristics. Furthermore, how to accurately control the dispersion properties to

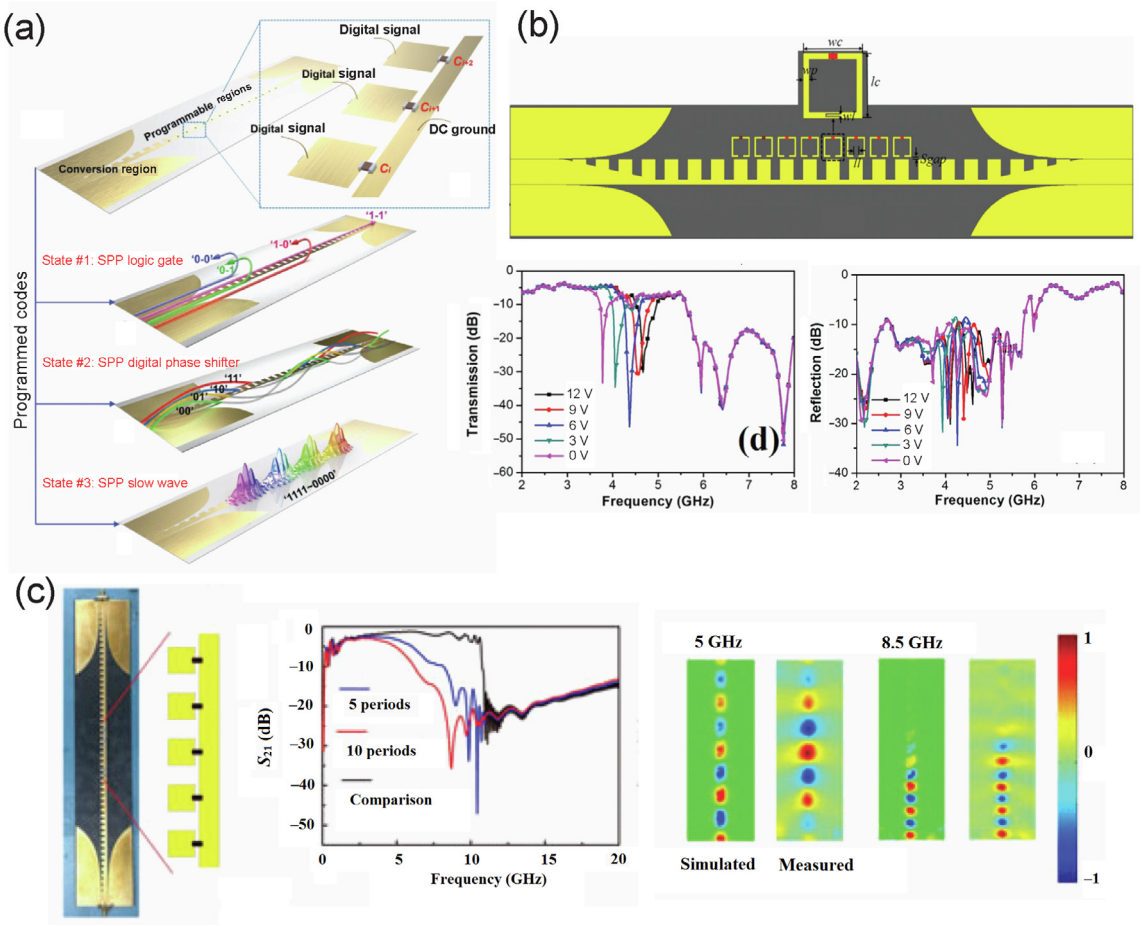

Fig. 8. Active tuning of SPPs. (a) Programmable designer SPP system composed of a designer SPP waveguide and the digital control, including the schematic of the programmable SPP waveguide and unit cells. And the programmable designer SPP system realizes three different digital analog functions. Reproduced with permission [41], Copyright (2017), Wiley-VCH. (b) The physical structure and measured results of transmission-spectrum-controllable structure based on the coupling between spoof SPPs TL and tunable metamaterial particles. Reproduced with permission [89], Copyright (2016), AIP. (c) The schematic, simulated S_{21} and measured field distributions of the SPP attenuator with ten complicated SPP units. Reproduced with permission [42], Copyright (2017), IEEE.

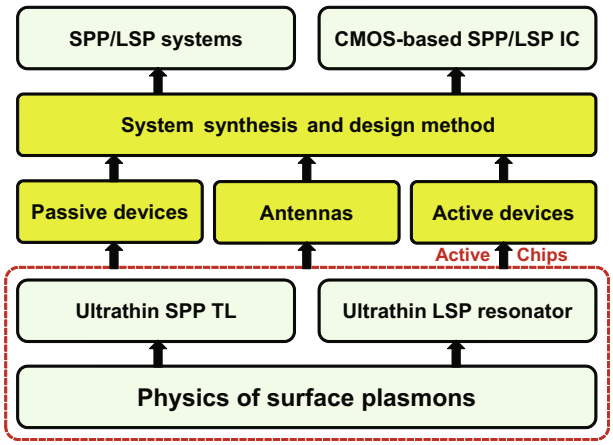

Fig. 9. (Color online) The current states of arts and future directions of spoof SPPs and LSPs in the microwave frequency.

design the required frequency responses? The synthesis and design method is also very useful for the study of CMOS-based SPP/LSP integrated circuits, which will have more impacts for the future information technologies. The current states of arts and future directions of spoof SPPs and LSPs at microwave frequencies are clearly illustrated in Fig. 9. Finally, we remark that the integration of spoof SPP/LSP devices with traditional microwave components so as to form hybrid circuits and systems with optimized performance is also a challenging task we need to tackle.

Thus far, SPP devices have been developed well at microwave frequencies but still insufficiently at THz frequency range, due to the lack of efficient THz sources and detectors. The realization of future compact THz integrated plasmonic circuits require the development of integration of a number of key components, such as high power THz source, high-speed modulators, low cross-talk TLs, fast tunable antennas, etc. Recently, a THz spoof SPP waveguide consisting of periodic metallic rectangular pillars have been experimentally realized and a series of waveguide components, including an S-bend, a Y-splitter, and directional couplers, have been developed [92]. We anticipate the growth of interests on THz spoof SPPs and further advancement of on-chip THz interconnects based on spoof SPPs reported in the future.

Conflict of interest

The authors declare that they have no conflict of interest.

Acknowledgments

This work was supported in part from the National Natural Science Foundation of China (61871127, 61735010, 61631007, 61571117, 61501112, 61501117, 61522106, 61722106, 61701107, 61701246 and 61701108), the Fundamental Research Funds for the Central Universities (2242018R30001), National Key Research and Development Program of China (2017YFA0700201, 2017YFA0700202, and 2017YFA0700203), and the 111 Project (111-2-05).

Author contributions

All authors contributed to the draft preparation; J. Z organized the materials, reviewed and edited the manuscript; T. J. C. administrated the project.

References

[1] Saxler J, Rivas JG, Janke C, et al. Time-domain measurements of surface plasmon polaritons in the terahertz frequency range. Phys Rev B 2004;69:155427.
[2] Wang KL, Mittleman DM. Metal wires for terahertz wave guiding. Nature 2004;432:376–9.
[3] Jeon TI, Grischkowsky D. THz Zenneck surface wave (THz surface plasmon) propagation on a metal sheet. Appl Phys Lett 2006;88:061113.
[4] Goubau G. Surface waves and their application to transmission lines. J Appl Phys 1950;21:1119–28.
[5] Mills DL, Maradudin AA. Surface corrugation and surface-polariton binding in the infrared frequency-range. Phys Rev B 1989;39:1569–74.
[6] Pendry JB, Martin-Moreno L, Garcia-Vidal FJ. Mimicking surface plasmons with structured surfaces. Science 2004;305:847–8.
[7] Martin-Cano D, Nesterov ML, Fernandez-Dominguez AI, et al. Domino plasmons for subwavelength terahertz circuitry. Opt Express 2010;18:754–64.
[8] Shen XP, Cui TJ, Martin-Cano D, et al. Conformal surface plasmons propagating on ultrathin and flexible films. Proc Natl Acad Sci USA 2013;110:40–5.
[9] Liu XY, Zhu L, Wu QS, et al. Highly-confined and low-loss spoof surface plasmon polaritons structure with periodic loading of trapezoidal grooves. AIP Adv 2015;5:077123.
[10] Zhou SY, Lin JY, Wong SW, et al. Spoof surface plasmon polaritons power divider with large Isolation. Sci Rep 2018;8:5947.
[11] Kianinejad A, Chen ZN, Zhang L, et al. Spoof plasmon-based slow-wave excitation of dielectric resonator Antennas. IEEE T Antenn Propag 2016;64:2094–9.
[12] Liu LL, Li Z, Xu BZ, et al. Dual-band trapping of spoof surface plasmon polaritons and negative group velocity realization through microstrip line with gradient holes. Appl Phys Lett 2015;107:201602.
[13] Zhang HC, Fan YF, Guo J, et al. Second-Harmonic generation of spoof surface plasmon polaritons using nonlinear plasmonic metamaterials. ACS Photonics 2016;3:139–46.
[14] Garcia-Vidal FJ, Martin-Moreno L, Pendry JB. Surfaces with holes in them: new plasmonic metamaterials. J Opt A-Pure Appl Opt 2005;7:S97–S101.
[15] Zhao WS, Eldaiki OM, Yang RX, et al. Deep subwavelength waveguiding and focusing based on designer surface plasmons. Opt Express 2010;18:21498–503.
[16] Zhu WQ, Agrawal A, Nahata A. Planar plasmonic terahertz guided-wave devices. Opt Express 2008;16:6216–26.
[17] Li Z, Liu LL, Sun HY, et al. Effective surface plasmon polaritons induced by modal dispersion in a waveguide. Phys Rev Appl 2017;7:044028.
[18] Hibbins AP, Evans BR, Sambles JR. Experimental verification of designer surface plasmons. Science 2005;308:670–2.
[19] Williams CR, Andrews SR, Maier SA, et al. Highly confined guiding of terahertz surface plasmon polaritons on structured metal surfaces. Nat Photonics 2008;2:175–9.
[20] Gao Z, Xu H, Gao F, et al. Surface-wave pulse routing around sharp right angles. Phys Rev Appl 2018;9:044019.
[21] Wan X, Shen XP, Luo Y, et al. Planar bifunctional Luneburg-fisheye lens made of an anisotropic metasurface. Laser Photon Rev 2014;8:757–65.
[22] Shen XP, Cui TJ. Planar plasmonic metamaterial on a thin film with nearly zero thickness. Appl Phys Lett 2013;102:211909.
[23] Ma HF, Shen XP, Cheng Q, et al. Broadband and high-efficiency conversion from guided waves to spoof surface plasmon polaritons. Laser Photon Rev 2014;8:146–51.
[24] Xu JJ, Zhang HC, Zhang Q, et al. Efficient conversion of surface-plasmon-like modes to spatial radiated modes. Appl Phys Lett 2015;106:021102.
[25] Xu J, Cui YJ, Guo J, et al. Broadband transition between microstrip line and spoof SP waveguide. Electron Lett 2016;52:1694-1681.
[26] Kianinejad A, Chen ZN, Qiu CW. Design and modeling of spoof surface plasmon modes-based microwave slow-wave transmission line. IEEE Trans Microw Theory Tech 2015;63:1817–25.
[27] Liu LL, Li Z, Gu CQ, et al. Smooth bridge between guided waves and spoof surface plasmon polaritons. Opt Lett 2015;40:1810–3.
[28] Liang Y, Yu H, Wen JC, et al. On-chip sub-terahertz surface plasmon polariton transmission lines with mode converter in CMOS. Sci Rep 2016;6:30063.
[29] Zhang HC, Cui TJ, Zhang Q, et al. Breaking the challenge of signal integrity using time-domain spoof surface plasmon polaritons. ACS Photon 2015;2:1333–40.
[30] Zhang HC, Zhang Q, Liu JF, et al. Smaller-loss planar SPP transmission line than conventional microstrip in microwave frequencies. Sci Rep 2016;6:23396.
[31] Tang WX, Zhang HC, Liu JF, et al. Reduction of radiation loss at small-radius bend using spoof surface plasmon polariton transmission line. Sci Rep 2017;7:41077.
[32] Zhang HC, Tang WX, Xu J, et al. Reduction of shielding-box volume using SPP-like transmission lines. IEEE Trans Compon Pack Manuf Technol 2017;7:1486–92.
[33] Wu JJ, Hou DJ, Liu KX, et al. Differential microstrip lines with reduced crosstalk and common mode effect based on spoof surface plasmon polaritons. Opt Express 2014;22:26777–87.
[34] Liang Y, Yu H, Zhang HC, et al. On-chip sub-terahertz surface plasmon polariton transmission lines in CMOS. Sci Rep 2015;5:14853.
[35] Liu LL, Li Z, Xu BZ, et al. Ultra-low-loss high-contrast gratings based spoof surface plasmonic waveguide. IEEE Trans Microw Theory Tech 2017;65:2008–18.
[36] Yang YH, Chen HS, Xiao SS, et al. Ultrathin 90-degree sharp bends for spoof surface plasmon polaritons. Opt Express 2015;23:19074–81.

[37] Wan X, Cui TJ. Guiding spoof surface plasmon polaritons by infinitely thin grooved metal strip. AIP Adv 2014;4:047137.
[38] Kianinejad A, Chen ZN, Qiu CW. Low-loss spoof surface plasmon slow-wave transmission lines with compact transition and high isolation. IEEE Trans Microw Theory Tech 2016;64:3078–86.
[39] Kianinejad A, Chen ZN, Qiu CW. Full modeling, loss reduction, and mutual coupling control of spoof surface plasmon-based meander slow wave transmission Lines. IEEE Trans Microw Theory Tech 2018;66:3764–72.
[40] Li Z, Sun YH, Wang KA, et al. Tuning the dispersion of effective surface plasmon polaritons with multilayer systems. Opt Express 2018;26:4686–97.
[41] Zhang HC, Cui TJ, Xu JE, et al. Real-time controls of designer surface plasmon polaritons using programmable plasmonic metamaterial. Adv Mater Technol 2017;2:1600202.
[42] Zhang XR, Zhang HC, Tang WX, et al. Loss analysis and engineering of spoof surface plasmons based on circuit topology. IEEE Antennas Wirel Propag Lett 2017;16:3204–7.
[43] Zhang XR, Tang WX, Zhang HC, et al. A spoof surface plasmon transmission line loaded with varactors and short-circuit stubs and its application in wilkinson power dividers. Adv Mater Technol 2018;3:1800046.
[44] Gao Z, Gao F, Zhang YM, et al. Forward/backward switching of plasmonic wave propagation using sign-reversal coupling. Adv Mater 2017;29:1700018.
[45] Tang XL, Zhang QF, Hu SM, et al. Capacitor-loaded spoof surface plasmon for flexible dispersion control and high-selectivity filtering. IEEE Microw Wirel Compon Lett 2017;27:806–8.
[46] Goubau G. On the excitation of surface waves. Proc Inst Radio Eng 1952;40:865–8.
[47] Pors A, Moreno E, Martin-Moreno L, et al. Localized spoof plasmons arise while texturing closed surfaces. Phys Rev Lett 2012;108:223905.
[48] Mayer KM, Hafner JH. Localized surface plasmon resonance sensors. Chem Rev 2011;111:3828–57.
[49] Luo Y, Lei DY, Maier SA, et al. Broadband light harvesting nanostructures robust to edge bluntness. Phys Rev Lett 2012;108:023901.
[50] Luo Y, Lei DY, Maier SA, et al. Transformation-optics description of plasmonic nanostructures containing blunt edges/corners: from symmetric to asymmetric edge rounding. ACS Nano 2012;6:6492–506.
[51] Shen XP, Cui TJ. Ultrathin plasmonic metamaterial for spoof localized surface plasmons. Laser Photonics Rev 2014;8:137–45.
[52] Li Z, Liu LL, Gu CQ, et al. Multi-band localized spoof plasmons with texturing closed surfaces. Appl Phys Lett 2014;104:101603.
[53] Huidobro PA, Shen XP, Cuerda J, et al. Magnetic localized surface plasmons. Phys Rev X 2014;4:021003.
[54] Liao Z, Luo Y, Fernandez-Dominguez AI, et al. High-order localized spoof surface plasmon resonances and experimental verifications. Sci Rep 2015;5:9590.
[55] Liao Z, Fernandez-Dominguez AI, Zhang JJ, et al. Homogenous metamaterial description of localized spoof plasmons in spiral geometries. ACS Photonics 2016;3:1768–75.
[56] Zhang JJ, Liao Z, Luo Y, et al. Spoof plasmon hybridization. Laser Photonics Rev 2017;11:1600191.
[57] Huang Y, Zhang JJ, Cui TJ, et al. Revealing the physical mechanisms behind large field enhancement in hybrid spoof plasmonic systems. J Opt Soc Am B 2018;35:396–401.
[58] Gao F, Gao Z, Luo Y, et al. Invisibility dips of near-field energy transport in a spoof plasmonic metadimer. Adv Funct Mater 2016;26:8307–12.
[59] Liao Z, Shen XP, Pan BC, et al. Combined system for efficient excitation and capture of LSP resonances and flexible control of SPP transmissions. ACS Photon 2015;2:738–43.
[60] Li Z, Xu J, Chen C, et al. Coplanar waveguide wideband band-stop filter based on localized spoof surface plasmons. Appl Optics 2016;55:10323–8.
[61] Xu BZ, Li Z, Liu LL, et al. Bandwidth tunable microstrip band-stop filters based on localized spoof surface plasmons. J Opt Soc Am B 2016;33:1388–91.
[62] Gao F, Gao Z, Zhang YM, et al. Vertical transport of subwavelength localized surface electromagnetic modes. Laser Photonics Rev 2015;9:571–6.
[63] Aubry A, Lei DY, Maier SA, et al. Interaction between plasmonic nanoparticles revisited with transformation optics. Phys Rev Lett 2010;105:233901.
[64] Gao F, Gao Z, Shi XH, et al. Dispersion-tunable designer-plasmonic resonator with enhanced high-order resonances. Opt Express 2015;23:6896–902.
[65] Zhao SM, Zhang HC, Zhao JH, et al. An ultra-compact rejection filter based on spoof surface plasmon polaritons. Sci Rep 2017;7:10576.
[66] Pan BC, Liao Z, Zhao J, et al. Controlling rejections of spoof surface plasmon polaritons using metamaterial particles. Opt Express 2014;22:13940–50.
[67] Yin JY, Ren J, Zhang HC, et al. Capacitive-coupled series spoof surface plasmon polaritons. Sci Rep 2016;6:24605.
[68] Zhang Q, Zhang HC, Yin JY, et al. A series of compact rejection filters based on the interaction between spoof SPPs and CSRRs. Sci Rep 2016;6:28256.
[69] Luo J, He J, Apriyana A, et al. Tunable surface-plasmon-polariton filter constructed by corrugated metallic line and high permittivity material. IEEE Access 2018;6:10358–64.
[70] Zhang Q, Zhang HC, Wu H, et al. A hybrid circuit for spoof surface plasmons and spatial waveguide modes to reach controllable band-pass filters. Sci Rep 2015;5:16531.
[71] Zhang X, Bao D, Liu JF, et al. Wide-bandpass filtering due to multipole resonances of spoof localized surface plasmons. Ann Der Phys 2018;530:1800207.
[72] Hu MZ, Zhang HC, Yin JY, et al. Ultra-wideband filtering of spoof surface plasmon polaritons using deep subwavelength planar structures. Sci Rep 2016;6:37605.
[73] Guan DF, You P, Zhang QF, et al. Hybrid spoof surface plasmon polariton and substrate integrated waveguide transmission line and its application in filter. IEEE Trans Microw Theory Tech 2017;65:4925–32.
[74] Wang J, Zhao L, Hao ZC, et al. An ultra-thin coplanar waveguide filter based on the spoof surface plasmon polaritons. Appl Phys Lett 2018;113:071101.
[75] Liu XY, Zhu L, Feng YJ. Spoof surface plasmon-based bandpass filter with extremely wide upper stopband. Chin Phys B 2016;25:034101.
[76] Gao X, Zhou L, Yu XY, et al. Ultra-wideband surface plasmonic Y-splitter. Opt Express 2015;23:23270–7.
[77] Wu YL, Li MX, Yan GY, et al. Ghassemlooy, single-conductor co-planar quasi-symmetry unequal power divider based on spoof surface plasmon polaritons of bow-tie cells. AIP Adv 2016;6:105110.
[78] Liu XY, Feng YJ, Chen K, et al. Planar surface plasmonic waveguide devices based on symmetric corrugated thin film structures. Opt Express 2014;22:20107–16.
[79] Gao X, Shi JH, Shen XP, et al. Ultrathin dual-band surface plasmonic polariton waveguide and frequency splitter in microwave frequencies. Appl Phys Lett 2013;102:151912.
[80] Kong GS, Ma HF, Cai BG, et al. Continuous leaky-wave scanning using periodically modulated spoof plasmonic waveguide. Sci Rep 2016;6:29600.
[81] Yin JY, Ren J, Zhang Q, et al. Frequency-controlled broad-angle beam scanning of patch array fed by spoof surface plasmon polaritons. IEEE Tran Antenn Propag 2016;64:5181–9.
[82] Xu JJ, Yin JY, Zhang HC, et al. Compact feeding network for array radiations of spoof surface plasmon polaritons. Sci Rep 2016;6:22692.
[83] Yin JY, Ren J, Zhang L, et al. Microwave vortex-beam emitter based on spoof surface plasmon polaritons. Laser Photonics Rev 2018;12:1600316.
[84] Kianinejad A, Chen ZN, Qiu CW. A single-layered spoof-plasmon-mode leaky wave antenna with consistent gain. IEEE Tran Antenn Propag 2017;65:681–7.
[85] Han YJ, Li YF, Ma H, et al. Multibeam antennas based on spoof surface plasmon polaritons mode coupling. IEEE Tran Antenn Propag 2017;65:1187–92.
[86] Lv XM, Cao WQ, Zeng ZY, et al. A circularly polarized frequency beam-scanning antenna fed by a microstrip spoof SPP transmission Line. IEEE Antenn Wirel Propag Lett 2018;17:1329–33.
[87] Zhang HC, Liu S, Shen XP, et al. Broadband amplification of spoof surface plasmon polaritons at microwave frequencies. Laser Photonics Rev 2015;9:83–90.
[88] Liu LL, Wu L, Zhang JJ, et al. Backward phase matching for second harmonic generation in negative-index conformal surface plasmonic metamaterials. Adv Sci 2018;5:1800661.
[89] Xu J, Zhang HC, Tang WX, et al. Transmission-spectrum-controllable spoof surface plasmon polaritons using tunable metamaterial particles. Appl Phys Lett 2016;108:191906.
[90] Song K, Mazumder P. Active terahertz spoof surface plasmon polariton switch comprising the perfect conductor metamaterial. IEEE Tran Electron Dev 2009;56:2792–9.
[91] Liang Y, Yu H, Feng GY, et al. An energy- efficient and low-crosstalk sub-THz I/O by surface plasmonic polariton interconnect in CMOS. IEEE Trans Microwave Theory Tech 2017;65:2762.
[92] Zhang Y, Xu YH, Tian CX, et al. Terahertz spoof surface-plasmon-polariton subwavelength waveguide. Photon Res 2018;6:18–23.

Jingjing Zhang is a professor of Southeast University, China. Her research interests include metamaterials, designer surface plasmons, and nanoplasmonics.

Tie-Jun Cui received the Ph.D. degree from Xidian University, China in 1993. He was an Alexander von Humboldt Foundation Research Fellow at the University of Karlsruhe, Germany (2005–2007), a Postdoctoral Research Associate (1997–2000) and Research Scientist (2001–2002) at the University of Illinois at Urbana-Champaign, USA. In 2002, he joined the Department of Radio Engineering, Southeast University, China, as Cheung-Kong Professor. Currently he is the Principal Professor of Southeast University. His research interests include metamaterials, plasmonics in microwaves, and computational electromagnetics.